CHEMISTRY OF MATERIALS
Article

Chem. Mater. **2010,** *22,* 1071–1079 1071
DOI:10.1021/cm9020518

Defective Ni Perovskites as Cathode Materials in Intermediate-Temperature Solid-Oxide Fuel Cells: A Structure−Properties Correlation[†]

Shu-en Hou,[‡,⊥] José Antonio Alonso,*[,§,⊥] Shreyas Rajasekhara,[⊥] María Jesús Martínez-Lope,[§] María Teresa Fernández-Díaz,[‖] and John B. Goodenough[⊥]

[‡]*Engineering Research Center of Nano-Geo Materials of Ministry of Education, China University of Geosciences, Wuhan, 430074, China.,* [§]*Instituto de Ciencia de Materiales de Madrid, CSIC, Cantoblanco, E-28049 Madrid, Spain,* [‖]*Institute Laue-Langevin (ILL) 156X, F-38042 Grenoble Cedex 9, France, and* [⊥]*Materials Science & Engineering Program, The University of Texas at Austin, Austin, Texas, 78712*

Received July 7, 2009. Revised Manuscript Received October 7, 2009

Four oxides belonging to the perovskite series of nominal stoichiometry $LaNi_{1-x}Mo_xO_3$, $x = 0.10$, 0.15, 0.20, 0.25 (LNMO), have been tested as cathode materials for solid oxide fuel cells (SOFC). The electrodes were supported on a 300-μm-thick pellet of the electrolyte $La_{0.8}Sr_{0.2}Ga_{0.83}Mg_{0.17}O_{3-\delta}$ (LSGM) with Sr_2MgMoO_6 (SMMO) as the anode and LNMO as the cathode. The test fuel cells gave a maximum power density of 660 mW/cm^2 at 850 °C and 565 mW/cm^2 at 800 °C for the $x = 0.25$ cathode material and exhibited high cyclability and low cathodic overpotential losses with pure H_2 as fuel. All the cathode materials were characterized by X-ray diffraction (XRD) and electrical conductivity measurements while the test fuel cell cross-section was examined by scanning electron microscopy (SEM). The X-ray data indicate that all the cathode materials exhibit a perovskite phase with an additional impurity phase present in LNMO $x = 0.20, 0.25$ materials. Molybdenum (Mo)-poor LNMO $x = 0.10$ exhibits a purely metallic behavior in the 120−800 °C temperature range, while Mo-rich LNMO, $x = 0.15$, 0.20, and 0.25, are semiconducting. Additionally, analysis of in situ temperature-dependent neutron powder diffraction (NPD) data from LNMO $x = 0.20$ at 25 and 800 °C in air reveal that it possesses a rhombohedral structure ($R\bar{3}c$ space group) with a crystallographic formula $La_{0.98(1)}Ni_{0.88(3)}Mo_{0.12(3)}O_{2.78(3)}$ and a nominal oxidation state for Ni of 2.16+, which points to the presence of a Ni(III)/Ni(II) redox couple in the cathode materials at the working temperature of the cell (800 °C). The Ni(III)/Ni(II) redox energy at the top of the O 2p bands accounts for a good electronic conductivity of polaronic nature of approximately 30 $S \cdot cm^{-1}$ at 800 °C. NPD data also showed a measurable oxygen deficiency of approximately 0.2 oxygen atoms per formula unit exhibiting large thermal factors, which accounts for the good oxygen mobility expected in a mixed ion−electronic conductor (MIEC) oxide. The excellent properties of $LaNi_{1-x}Mo_xO_{3-\delta}$ cathodes, especially for $x = 0.25$, with long-term stability and low cathodic overpotential losses make them potential electrode materials for the first generation of cobalt-free intermediate-temperature SOFCs, with power densities exceeding the target of 500 mW/cm^2 at 800 °C in pure H_2 as a fuel.

1. Introduction

The solid oxide fuel cell (SOFC) system consisting of an anode, a cathode, and an electrolyte is an attractive concept for the generation of off-grid, distributed electric power or for a bottoming cycle of a conventional power plant because power output from SOFCs is not constrained by Carnot cycle limitations. However, manufacturing cost-competitive SOFCs with sufficient life, power output, and reliability at an operating temperature $T_{op} \approx 800$ °C still remains a challenge.

Currently SOFCs utilize a thin yttria-stabilized-zirconia (YSZ) electrolyte supported on a porous anode, with cathodes consisting of a perovskite system $La_{1-x}A_xMnO_{3+\delta}$ (A = Ca or Sr and $x \approx 0.2$).[1] It is a p-type, small-polaron conductor that is catalytically active for O_2 reduction, but it is a poor oxide-ion conductor. Therefore the final step of the reduction of O_2 to $2O^{2-}$ ions, which are subsequently transferred to the anode through the electrolyte, requires the transfer of oxygen from the reaction site on the $La_{1-x}A_xMnO_{3+\delta}$ surface to a triple-phase boundary (TPB) consisting of a cathode/YSZ/air interface. This condition introduces constraints on the optimum morphology of a composite YSZ/$La_{1-x}A_xMnO_{3+\delta}$ electrolyte−cathode system.

Electrode materials are also limited by overpotential (polarization) losses as current flowing through them increases. This loss consists of two components: (1) a

[†] Accepted as part of the 2010 "Materials Chemistry of Energy Conversion Special Issue".
*Corresponding author. E-mail: ja.alonso@icmm.csic.es.

(1) Huang, K. Solid Oxide Fuel Cells. In *Materials for Fuel Cells*; Gsik, M., Ed.; Woodhead Publishing Ltd: Cambridge, 2009; Chapter 8.

© 2009 American Chemical Society

"concentration polarization" due to slow diffusion of the gaseous reactant, that is, O_2 at the cathode, into the electrode pores, and (2) an "activation polarization" related to the activation energies for the reduction of O_2 to $2O^{2-}$ ions at the cathode and their transfer to the electrolyte. An anode-supported electrolyte allows the $La_{1-x}A_xMnO_{3+\delta}$ cathode to be made thin enough for the activation polarization to be rate-limiting, but even then the activation polarization of $La_{1-x}A_xMnO_{3+\delta}$ cathode materials is too large for the cathode to be viable at a T_{op} < 800 °C.

An alternative approach for better cathode materials is to use an oxide that is a mixed O^{2-}-ion/electronic conductor (MIEC) and is catalytically active for O_2 reduction to $2O^{2-}$ in which transfer of the surface O^{2-} ion is to the electrolyte through the cathode bulk. With such an oxide, the O^{2-} ions can traverse a thin electrode to the electrolyte from reaction sites over the entire surface area of the cathode; the active reaction sites are not restricted to those near a TPB. With a metallic mesh contacting the cathode surface to deliver electrons to near the reaction sites, the electronic conduction in an MIEC is not rate-limiting. To date, the search for an MIEC that is mixed-valent, has a thermal expansion matched to that of the electrolyte, and contains mobile oxygen vacancies in the oxidizing atmosphere of the cathode has concentrated on transition-metal oxides having an active redox couple pinned at the top of the O 2p bands, that is, Fe(IV)/Fe(III), Co(IV)/Co(III), Ni(III)/Ni(II), Ni(IV)/Ni(III), and Cu(III)/Cu(II). Specifically, good oxygen-vacancy mobility in the oxoperovskites has led to extensive investigation of $LaFeO_3$, $LaCoO_3$, and/or $LaNiO_3$ perovskites doped with Sr or Ca.[2−6] The best of these MIEC cathodes has been $La_{1-x}Sr_xFe_{1-y}Co_yO_{3-\delta}$ with x and y chosen to give the largest δ at T_{op} compatible with an acceptable match of the thermal expansion to that of the electrolyte.[7,8] The Co(IV)/Co(III) couple in the $La_{1-x}Sr_xFe_{1-y}Co_yO_{3-\delta}$ system has the lowest activation polarization loss; dilution of cobalt sites with iron reduces the thermal expansion associated with low-spin to high-spin transitions on the Co(III) ions and reduces the cobalt content of this system. Even with low cobalt content, this cathode material is too expensive for a SOFC system to be cost-competitive. As a reference, the relative costs of Co, Ni, Mn, and Fe oxides are, roughly, 10:6:2:1. Replacing Co by Ni oxides involves a saving of about 40% in the cathode material.

Here we report on a cobalt-free Mo-doped $LaNiO_3$ MIEC cathode of acceptable activation polarization loss at 800 °C in SOFC with a $La_{0.8}Sr_{0.2}Ga_{0.83}Mg_{0.17}O_{3-\delta}$ (LSGM) electrolyte and a double perovskite $Sr_2MgMoO_{6-\delta}$ (SMMO) anode; power densities of approximately 565 mW/cm^2 at 800 °C were obtained with H_2 as fuel. We discuss the rationale for choosing this cathode system and the possible reasons for superior performance of this cathode material.

(2) Guo, W. M.; Lin, J.; Jin, C.; Gao, H. B.; Zhang, Y. H. *J. Alloys Compd.* **2009**, *473*, 43.
(3) Lin, Y.; Barnett, S. A. *Solid State Ionics* **2008**, *179*, 420.
(4) Bidrawn, F.; Lee, S.; Vohs, J. M.; Gorte, R. J. *J. Electrochem. Soc.* **2008**, *155*, B660.
(5) Hsu, M. F.; Wu, L. J.; Wu, J. M.; Shiu, Y. H.; Lin, K. F. *Electrochem. Solid State Lett.* **2006**, *9*, A193.
(6) Huang, K. Q.; Feng, M.; Goodenough, J. P.; Milliken, C. *J. Electrochem. Soc.* **1997**, *114*, 3620.
(7) Tai, L.-W.; Nasrallah, M. M.; Anderson, H. U.; Sparlin, D. M.; Sehlin, S. R. *Solid State Ionics* **1995**, *76*, 273.
(8) Tai, L.-W.; Nasrallah, M. M.; Anderson, H. O. *J. Solid State Chem.* **1995**, *118*, 117.

2. Experimental Section

Nominal $LaNi_{1-x}Mo_xO_3$ (LNMO) materials were obtained for x = 0.10 and 0.15 in polycrystalline form by a citrate technique. Stoichiometric amounts of analytical grade La_2O_3, $Ni(NO_3)_2\cdot 6H_2O$, and $(NH_4)_6Mo_7O_{24}\cdot 4H_2O$ were dissolved in citric acid; the citrate solution was slowly evaporated, leading to an organic resin that was dried and decomposed by slowly heating up to 600 °C in air for 12 h. This treatment gave rise to highly reactive precursor materials that were finally heated at 800 and 1000 °C for 12 h each. The x = 0.20 and 0.25 samples were obtained by a standard ceramic procedure, mixing and grinding stoichiometric amounts of the above-mentioned reactants, heating the mixtures in air at 800 °C and 1000 °C and two times at 1200 °C for 20 h each, in alumina crucibles, with intermediate grindings. The reaction products were characterized by powder X-ray diffraction (XRD) for phase identification and to assess phase purity. The characterization was performed with a Philips X'pert diffractometer (40 kV, 30 mA) in Bragg−Brentano reflection geometry with Cu Kα radiation (λ = 1.5418 Å).

The crystal structure of the x = 0.20 sample was studied in situ in air by neutron powder diffraction (NPD) in the D1A diffractometer at the Institute Laue Langevin (ILL)—Grenoble at room temperature (RT) and at the working temperature of the SOFC (800 °C). The high-intensity mode ($\Delta d/d \geq 2 \times 10^{-3}$) was selected with a neutron wavelength λ = 1.91 Å over the angular range $0.1° < 2\theta < 150°$ with a 0.05° step. For the RT collection, approximately 2 g of sample were contained in a vanadium sample holder. For the high-temperature experiment, the sample was loaded into a quartz tube open at ambient atmosphere and placed in the isothermal zone of a furnace with a vanadium resistor operating under vacuum ($P_{O2} \approx 10^{-6}$ Torr). The collection time was 5 h in both cases. The NPD patterns were analyzed by the Rietveld method[9] with the Fullprof program.[10] A pseudo-Voigt function was used to generate the profile shape. The irregular background coming from the quartz container was interpolated from points devoid of reflections. The coherent scattering lengths used for La, Ni, Mo, and O were 8.24, 10.300, 6.715, and 5.803 fm, respectively.

The electrical conductivity measurements were performed from 120 to 800 °C in air with the dc four-probe method. For this purpose, cylindrical pellets of 6.50 mm diameter and 8.0 mm length were sintered at 1100 °C for x = 0.10 and 0.15 and at 1200 °C for x = 0.20 and 0.25 for 10 h. Platinum (Pt) wires and Pt paste were used to make the four probes. A current load of 10−100 mA was applied with a Keithley 224 current source, and the corresponding voltage drop was recorded with a HP3478A voltmeter.

Single-cell tests were performed on electrolyte-supported cells with $La_{0.8}Sr_{0.2}Ga_{0.83}Mg_{0.17}O_{3-\delta}$ (LSGM) as the electrolyte. LSGM pellets of 20-mm diameter were sintered at 1450 °C for 20 h and then polished with a diamond-coated wheel to a thickness of 300 μm. The anode was the double perovskite

(9) Rietveld, H. M. *J. Appl. Crystallogr.* **1969**, *2*, 65.
(10) Rodríguez-Carvajal, J. *Physica B* **1993**, *192*, 55.

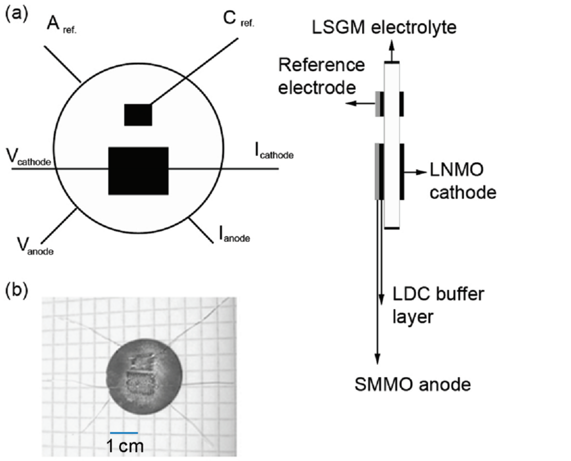

Figure 1. (a) Plan view and schematic cross-section of the test fuel cell used for the experiments. (b) Plan view image of the cathodic side of an actual fuel cell used in one of our experiments.

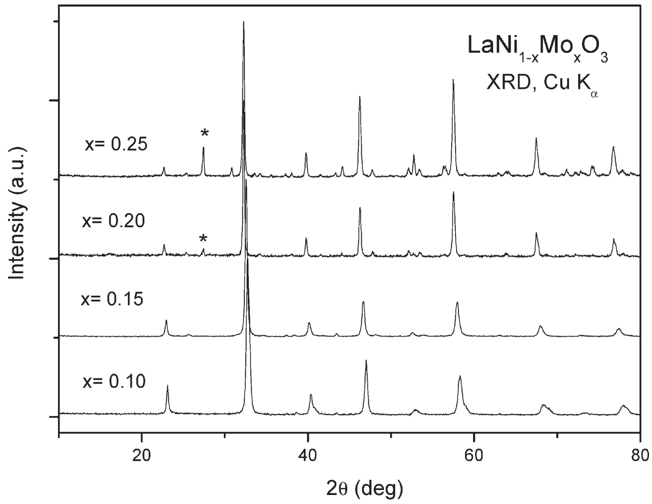

Figure 2. XRD patterns of $LaNi_{1-x}Mo_xO_{3-\delta}$ (x = 0.20, 0.25). The star indicates the most intense reflection of the La_2MoO_6 impurity.

$Sr_2MgMoO_{6-\delta}$ (SMMO) prepared by a sol–gel technique as described elsewhere.[11] A $La_{0.4}Ce_{0.6}O_{2-\delta}$ (LDC) buffer layer was deposited between the anode and the electrolyte to prevent the interdiffusion of ionic species between perovskite and electrolyte. Inks of LDC, SMMO, and LNMO were prepared with a binder (V-006 from Heraeus). LDC ink was screen-printed onto one side of the LSGM disk followed by a thermal treatment at 1300 °C in air for 1 h. SMMO was subsequently screen printed onto the LDC layer and fired at 1275 °C in air. Finally, LNMO was screen printed onto the other side of the disk and fired at 1100 °C (for x = 0.10 and 0.15) and 1200 °C (for x = 0.20 and 0.25) for 1 h. The working electrode area of the cell was 0.24 cm^2 (0.6 × 0.4 cm). Reference electrodes of the same materials as the working electrodes were used to monitor the overpotential losses of the cathode and anode in the cell configuration (Figure 1). A Pt-gauze current collector was carefully glued on both the anodic and the cathodic sides to ensure electrical contact by applying intermittent daubs of Pt paste between the Pt gauze and the electrode material. The cells were tested in a vertical tubular furnace at 750, 800, and 850 °C where the anode side was fed with a flow of pure H_2 (20 mL/min) and the cathode operated in an air flow of approximately 100 mL/min. The electrochemical parameters were measured with an EG&G Princeton Applied Research Potentiostat-Galvanostat, model 273.

Micrographs of cross-sectional layers from the SMMO/LDC/LSGM/LNMO cells were taken with a SEM (JEOL JSM-5610).

3. Results

3.1. X-ray Diffraction (XRD). Room temperature XRD patterns of $LaNi_{1-x}Mo_xO_3$ (x = 0.10, 0.15, 0.20, 0.25) all exhibit perovskite phases (Figure 2), with the La_2MoO_6 impurity phase first appearing in x = 0.20 and increasing in quantity for x = 0.25. As a first approach, the crystal structure of the main perovskite phases could be defined from the XRD data in a $GdFeO_3$ structural type (space group *Pbnm*) with the unit-cell parameters listed in Table 1. These results are in agreement with the findings of Rodriguez et al.[12] who first reported the

Table 1. Unit-Cell Parameters for $LaNi_{1-x}Mo_xO_{3-\delta}$, Refined from XRD Data at RT in the Orthorhombic Space Group *Pbnm*

nominal x	*a* (Å)	*b* (Å)	*c* (Å)	*V* (Å^3)
0.10	5.454(1)	5.512(1)	7.780(2)	233.86(8)
0.15	5.523(3)	5.526(3)	7.8048(3)	238.2(2)
0.20	5.547(1)	5.553(1)	7.833(1)	241.3(1)
0.25	5.5473(8)	5.5637(8)	7.863(1)	241.86(6)

preparation and structural characterization of the $LaNi_{1-x}Mo_xO_3$ perovskite series and described the formation of single-phase compounds for $x \leq 0.2$. Trials to introduce higher Mo content gave rise to the segregation of La_2MoO_6 as a secondary phase.[13] In the present study we confirm the formation of a perovskite phase for x = 0.25 with similar unit-cell parameters to those reported for $LaNi_{0.8}Mo_{0.2}O_3$,[12] namely, a = 5.547(1), b = 5.553(1), and c = 7.833(1) Å. The segregation of La_2MoO_6 suggests a certain departure of the nominal stoichiometry for the x = 0.20 and 0.25 phases, including the formation of La vacancies.

3.2. Neutron Powder Diffraction Thermo-Diffractometry Study. The refinement of the crystal structure of $LaNi_{0.80}Mo_{0.20}O_3$ from NPD data recorded at RT demonstrated that this sample contains two perovskite polymorphs: rhombohedral and orthorhombic. The rhombohedral phase was defined in the $R\bar{3}c$ space group (no. 167), Z = 6, with lattice parameters a = 5.5385(4), c = 13.541(2) Å, and V = 359.74(7) Å^3. La atoms are located at 1*b* positions, Ni and Mo are distributed at random over the 1*a* sites, and oxygen atoms are at 3*d* positions. The orthorhombic phase was defined in the space group *Pbnm* (No.62), Z = 4, with the $GdFeO_3$-type structure. The lattice parameters were a = 5.527(1) Å, b = 5.477(1) Å, c = 7.747(6) Å, and V = 234.5(2) Å^3. La atoms were located at 4*c* positions, Ni and Mo atoms distributed at random at 4*b* sites, and oxygen atoms at 4*c* and 8*d* positions. A satisfactory fit between the observed and the calculated profiles was obtained including

(11) Huang, Y.-H.; Dass, R. I.; Xing, Z.-L.; Goodenough, J. B. *Science* **2006**, *312*, 254.
(12) Rodriguez, E.; Alvarez, I.; López, M. L.; Veiga, M. L.; Pico, C.; Martínez, J. L. *J. Mater. Chem.* **2001**, *11*, 673.
(13) Xue, J. S.; Antonio, M. R.; Soderholm, L. *Chem. Mater.* **1995**, *7*, 333.

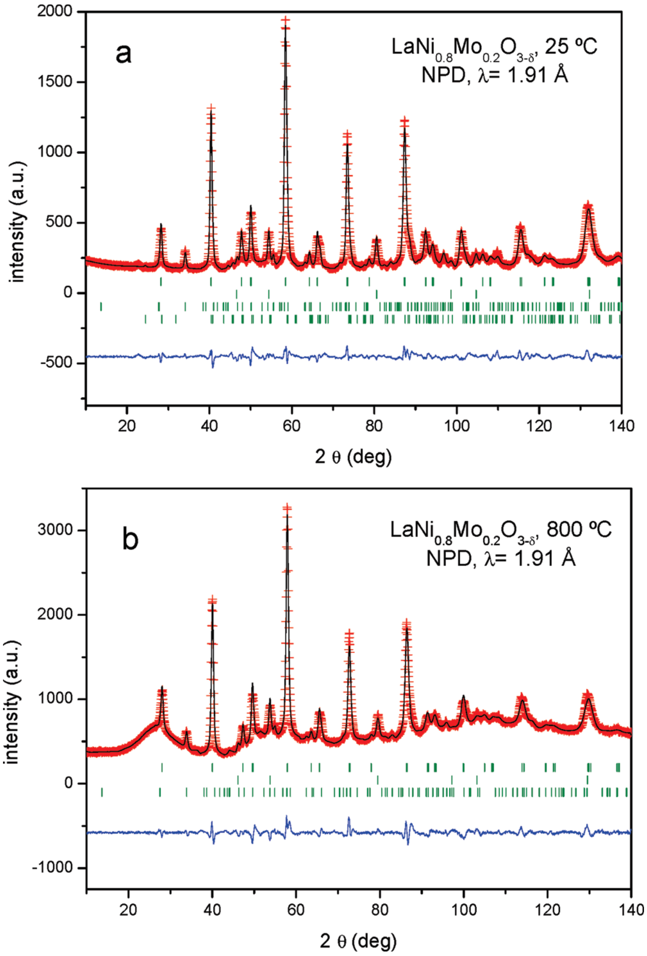

Figure 3. NPD Rietveld profiles of $LaNi_{0.8}Mo_{0.2}O_{3-\delta}$ at (a) 25 °C and (b) 800 °C. The main perovskite phase is defined in the $R\bar{3}c$ space group. The second and third series of Bragg reflections correspond to NiO and La_2MoO_6 impurities. The fourth series at 25 °C belong to a perovskite phase defined in the *Pbnm* space group.

La_2MoO_6 as a second phase defined in the $I4_1/acd$ space group[13] and NiO as a third phase with a rock-salt structure defined in $Fm\bar{3}m$ (Figure 3a). From the scale factors of the different phases, the relative molar amounts of rhombohedral and orthorhombic perovskites, La_2MoO_6, and NiO were determined to be 84(1)%, 3.9(1)%, 9.5(4)%, and 2.5(1)%, respectively.

The NPD pattern of $LaNi_{0.80}Mo_{0.20}O_3$ measured in situ at 800 °C in air is shown in Figure 3b. The irregular background arises from the quartz container required for high-temperature measurements as discussed earlier (Section 2). In this case the pattern contains only the rhombohedral polymorph with lattice parameters a = 5.5857(1), c = 13.6229(3) Å, and V = 368.09(1) Å^3, as well as La_2MoO_6 (9.5(5)%) and NiO (5.1(1)%). The refinement of 18 profile and atomic parameters resulted in a final residual R_{Bragg} = 2.68%.

Tables 2 and 3 contain the structural parameters and selected interatomic distances and angles of the main perovskite phases at 25 and 800 °C. A view of the rhombohedral superstructure is shown in Figure 4. From the values gathered in Table 2, we note large thermal factors for oxygen atoms at 800 °C of 2.9(1) Å^2, which may signify a dynamic disorder over the oxygen positions at this temperature. There is also a significant oxygen deficiency, already suggesting a higher mobility of oxygen in these partially occupied oxygen sites. Moreover, after the refinement of the mixed occupancy factors of Ni and Mo, the crystallographic formula $La_{0.984(6)}Ni_{0.88(3)}Mo_{0.12(3)}O_{2.78(2)}$ was obtained at 800 °C with a corresponding oxidation state of 2.16+ for the Ni cations. The NiO_6 octahedra are slightly distorted with O−Ni−O angles of 90.8° (25 °C) and 90.6° (800 °C) and (Ni,Mo)−O distances that increase from 1.981(1) Å at 25 °C to 1.989(1) Å at 800 °C. The mean tilting angle of the $(Ni,Mo)O_6$ octahedra, which controls the orbital overlap and hence the electronic transport properties, becomes more open as temperature increases, from 162.2° at RT to 164.7° at 800 °C, which favors the mentioned properties at high temperatures.

The thermal expansion coefficient (TEC) of $LaNi_{0.80}Mo_{0.20}O_{3-\delta}$ was determined to be 9.8 × 10^{-6} K^{-1} from the unit-cell volumes at 25 and 800 °C, which is significantly larger than that of $LaNiO_3$ (8.2 10^{-6} K^{-1}).[14]

Table 2. Structural Parameters for the Main Perovskite Phase of $LaNi_{0.8}Mo_{0.2}O_3$, Refined in the Rhombohedral $R\bar{3}c$ (No. 167) Space Group at 25 and 800 °C from NPD data

		temperature (K)	
		25	800
a (Å)		5.5387(4)	5.5870(6)
c (Å)		13.541(2)	13.642(3)
V (Å^3)		359.75(6)	368.8(1)
La	6a (0 0 1/4)		
f_{occ}		0.982(4)	0.984(6)
B (Å^2)		1.62(9)	2.6(1)
(Ni,Mo)	6b (0 0 0)		
B (Å^2)		0.63(7)	1.35(8)
f_{occ}(Ni)		0.12	0.12
O	18e (x 0 1/4)		
x		0.4447(3)	0.4527(5)
f_{occ}		0.908(1)	0.926(8)
B (Å^2)		1.14(9)	2.9(1)
	reliability factors		
χ^2		6.34	5.22
R_p (%)		3.48	2.60
R_{wp} (%)		4.52	3.61
R_I (%)		2.45	1.58

Table 3. Main Interatomic Distances (Å) and Selected Angles (deg) for $LaNi_{0.8}Mo_{0.2}O_3$ at 25 and 800 °C

	temperature (°C)	
	25	800
La−O	3.076(2)	3.058(3) ×3
	2.463(2)	2.529(1) ×3
	2.783(1)	2.800(3) ×8
(Ni,Mo)−O	1.981(1)	1.989(1) ×6
O−(Ni,Mo)−O	90.76(7)	90.6(1)
(Ni,Mo)−O−(Ni,Mo)	162.21(2)	164.74(3)
BVS[a] Ni	2.25(2)	2.27(1)
effective coordination	5.45	5.64

[a] The bond valences (BVS) for Ni cations have been calculated as BVS = $\sum_i \exp(r_i - r_0)/0.37$, where r_0 = 1.654 for the pair $Ni^{2+}-O^{2-}$ and r_i are the individual Ni−O distances of this table,[23,24] and taking into account the effective coordination of Ni cations.

(14) Touloukian, Y. S.; Kirby, R. K.; Taylor, R. E.; Lee, T. Y. R. *Thermal Expansion, Nonmetallic Solids, Thermophysical Properties of Matter*; Plenum: New York, 1977; Vol. *13*.

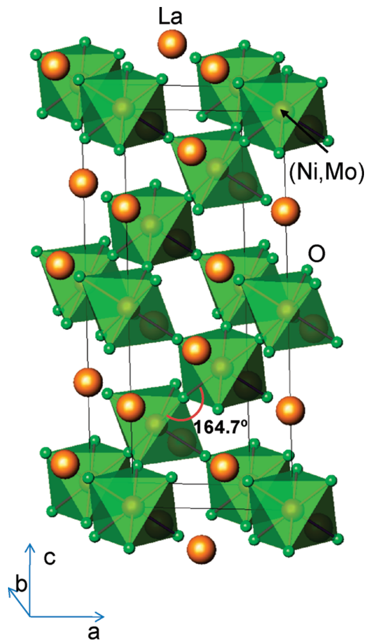

Figure 4. View of the crystal structure of $LaNi_{0.8}Mo_{0.2}O_{3-\delta}$ at 800 °C, defined as a $R\bar{3}c$ superstructure of perovskite consisting of a framework of slightly tilted $(Ni,Mo)O_6$ octahedra with La atoms in the voids.

3.3. Electronic Transport. Figure 5a shows the electronic conductivity σ as a function of temperature of LNMO for $x = 0.10$, 0.15, 0.20, and 0.25 from 120 to 800 °C in air atmosphere. The $x = 0.10$ compound exhibits an excellent conductivity of approximately 240 S cm^{-1} at 120 °C, which decreases upon heating to 800 °C displaying a metal-like behavior. For the remaining samples, a much lower conductivity is observed at 120 °C that increases with temperature, reaching approximately 40 S cm^{-1} for $x = 0.15$ and 30 S cm^{-1} for $x = 0.2$ and 0.25 at 800 °C (Figure 5a). The presence of a resistive impurity that may segregate in grain boundaries in the more-heavily doped samples probably contributes to the total conductivity, though not to the bulk conductivity. Interestingly, there is a crossover of the total conductivity of the two Mo-rich compounds at approximately 450 °C; at higher temperatures any grain boundary contribution would be much lower and thus the convergence of the conductivity of both samples. In any case, the performance of cell depends on the total conductivity; its influence on the electrochemical properties of the fuel cell are discussed in Section 4.

Assuming these oxides exhibit polaronic conduction in this temperature range that is governed by a small-polaron hopping mechanism,

$$\sigma = \frac{A}{T}\exp\left(-\frac{E_A}{kT}\right)$$

we plotted a graph of $\ln(\sigma T)$ vs $1/T$ (Figure 5b). A linear relationship is obtained, validating our assumption, and the polaron hopping activation energy E_A was estimated to be 0.104(1) eV for $x = 0.10$; 0.129(1) eV for $x = 0.15$; 0.154(1) eV for $x = 0.20$; and 0.152(1) for $x = 0.25$. Polaronic conduction in these materials implies the presence of a mixed valent Ni(III)/Ni(II) couple that facilitates good

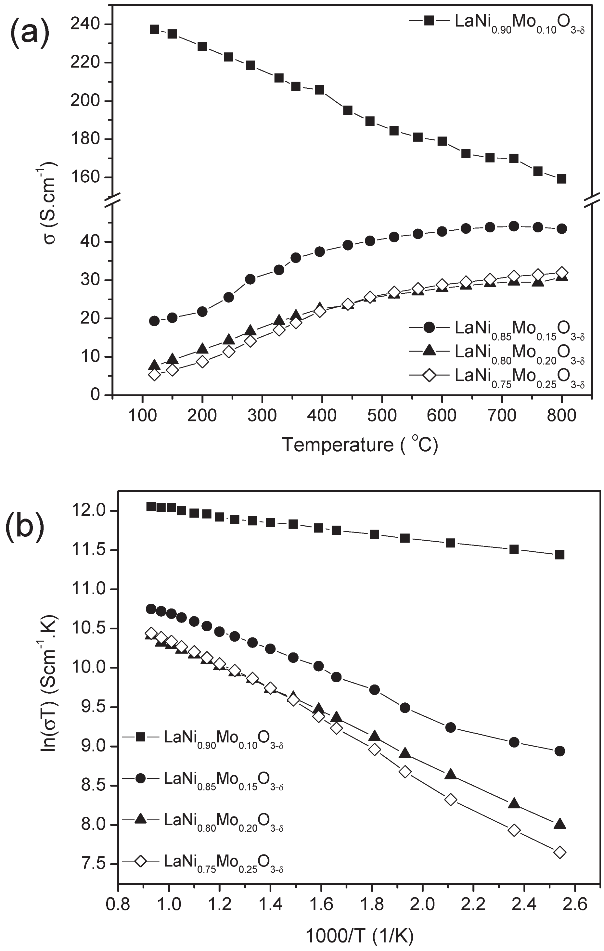

Figure 5. (a) Electrical conductivities of $LaNi_{1-x}Mo_xO_{3-\delta}$ ($x = 0.10$, 0.15, 0.20, and 0.25) measured in air in the 200−800 °C temperature range and (b) Arrehnius plot of the electrical conductivities of the LNMO family of materials.

electronic conduction at high temperatures. The systematic evolution of the activation energies suggests a narrowing of the Ni(III)/Ni(II) redox couple with increasing Mo concentration. Finally, thermoelectric measurements for the $x = 0.25$ material indicate that it is a p-type semiconductor above 350 K, confirming a hole-hopping conduction mechanism from Ni(III) to neighboring Ni(II) cations through Ni−O−Ni paths.

3.4. Cell Performance. Figures 6 and 7 show the cell voltage and power density as a function of the current density for the single fuel cells built with LNMO as cathode and SMMO as anode working in a pure H_2 flow. With $x = 0.10$ and 0.15 oxides (Figure 6a) as a cathode, the maximum power density (P_{max}) is poor at 800 °C, below 190 mW/cm^2. Moreover, the performance of the cathode in successive power cycles from open circuit voltage (OCV) to 0.4 V and back to OCV drops rapidly when cycled 50 times (Figure 6b). However, the maximum power density of LNMO cathodes with $x = 0.20$ increased to approximately 230 mW/cm^2 at 800 °C and 360 mW/cm^2 at 850 °C (Figure 7a). The performance of the cell built with the $x = 0.25$ cathode material was even better, reaching a P_{max} of 660 mW/cm^2 at 850 °C, 565 mW/cm^2 at 800 °C, and 270 mW/cm^2 at

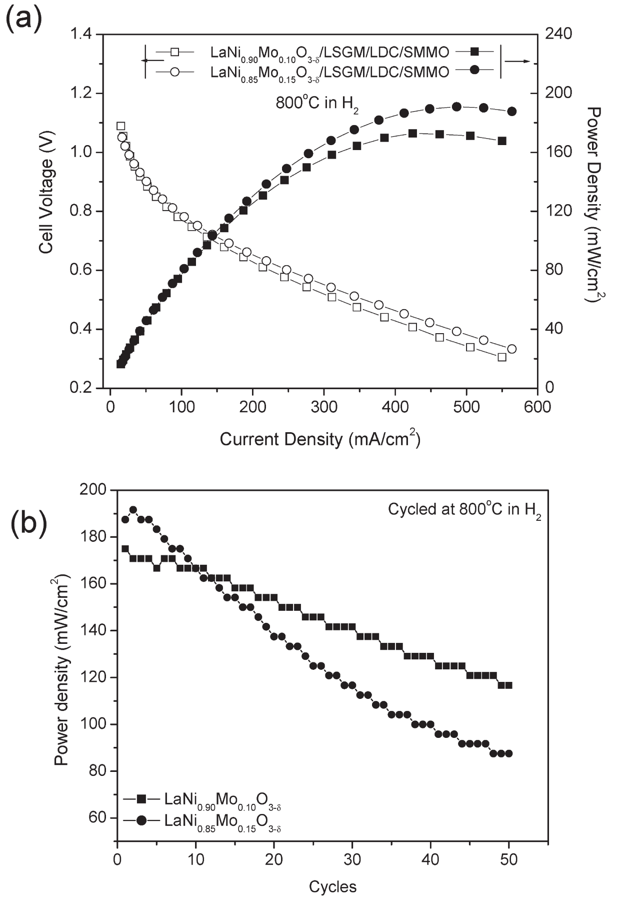

Figure 6. (a) Cell voltage (left axis) and power density (right axis) as a function of the current density for the test cell with $LaNi_{1-x}Mo_xO_{3-\delta}$ (x = 0.10 and 0.15) as a cathodic material. (b) Maximum power density as a function of number of cycles for SOFCs with $LaNi_{1-x}Mo_xO_{3-\delta}$ (x = 0.10 and 0.15).

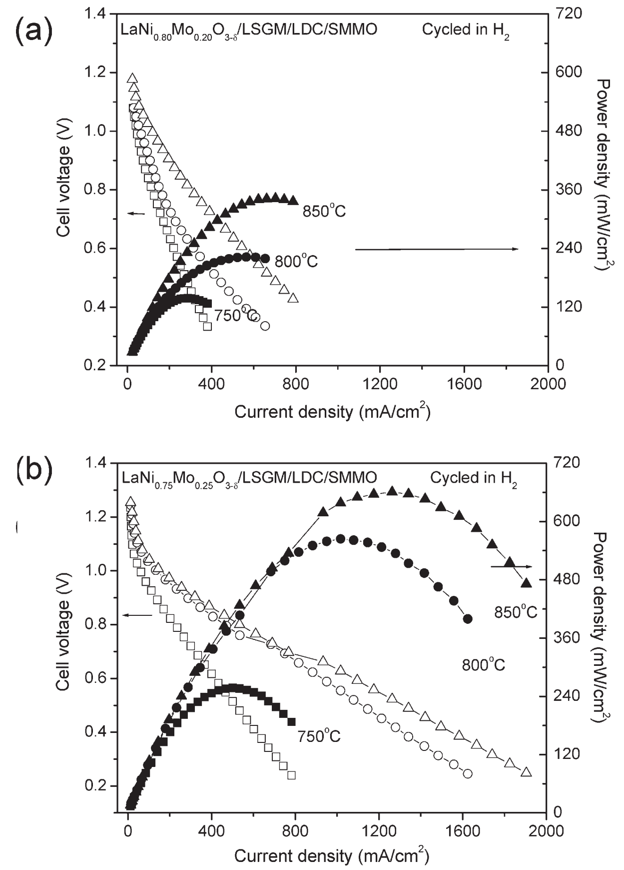

Figure 7. Cell voltage (left axis) and power density (right axis) as a function of the current density for (a) test cell with $LaNi_{0.80}Mo_{0.20}O_{3-\delta}$ as a cathodic material and (b) test cell with $La_{0.75}Mo_{0.25}O_{3-\delta}$ as a cathodic material.

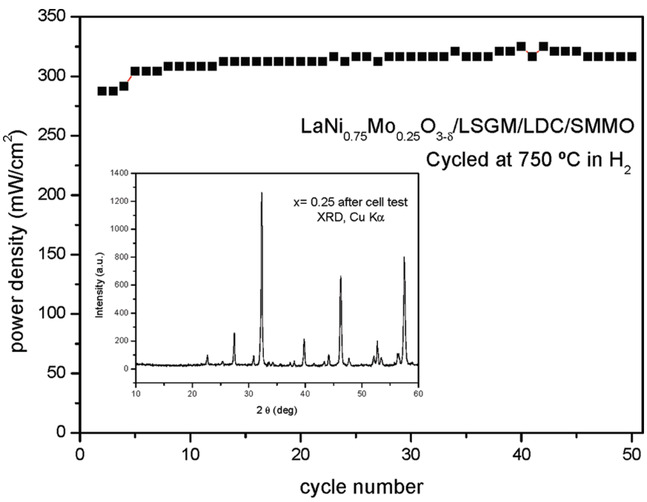

Figure 8. Stability of the test cell with $LaNi_{0.75}Mo_{0.25}O_3$ as a cathodic material versus number of cycles at 750 °C. The inset shows the XRD pattern of the cathode after the cell tests, corresponding to the perovskite phase, La_2MoO_6 and NiO.

750 °C (Figure 7b). The maximum power density at 800 °C is close to the often-considered target value of 500 mW/cm^2 for technological applications.[15] To test the stability of this cathode (LNMO x = 0.25), we ran successive power cycles at 750 °C, and the maximum power density did not degrade even after 50 cycles (Figure 8). Chemical stability was checked by XRD after the cell tests, showing no evidence of electrolyte−cathode reaction or cathode decomposition, as shown in the inset of Figure 8, where the XRD peaks correspond to the perovskite phase, La_2MoO_6, and NiO, as for the original sample.

The anode and cathode overpotentials, η_a and η_c, of x = 0.20 and x = 0.25 single cells operating at 800 °C are compared in Figure 9. Both cathode materials exhibit relatively low overpotential losses, which translates into higher power densities as is observed in our fuel-cell tests (Figure 7a,b). While the η_c is significantly lower than η_a for both cathode materials, the rate of overpotential increase as a function of current density is significantly lower for the x = 0.25 cathode material. At a current density of 500 mA/cm^2, LNMO x = 0.20 exhibits η_c of approximately 0.20 V whereas η_c for x = 0.25 is less than 0.10 V (Figure 9).

3.5. Scanning Microscopy. Figure 10 shows two representative micrographs of the cross sections of the test cells for x = 0.25. They show clear interfaces of LSGM/LNMO and LSGM/LDC/SMMO after testing in H_2. From the SEM images, the thicknesses of the LDC,

(15) Tarancón, A.; Morata, A.; dezanneau, G.; Skinner, S. J.; Kilner, J. A.; Estradé, S.; Hernández-Ramírez, F.; Peiró, F.; Morante, J. R. *J. Power Sources* **2007**, *174*, 255.

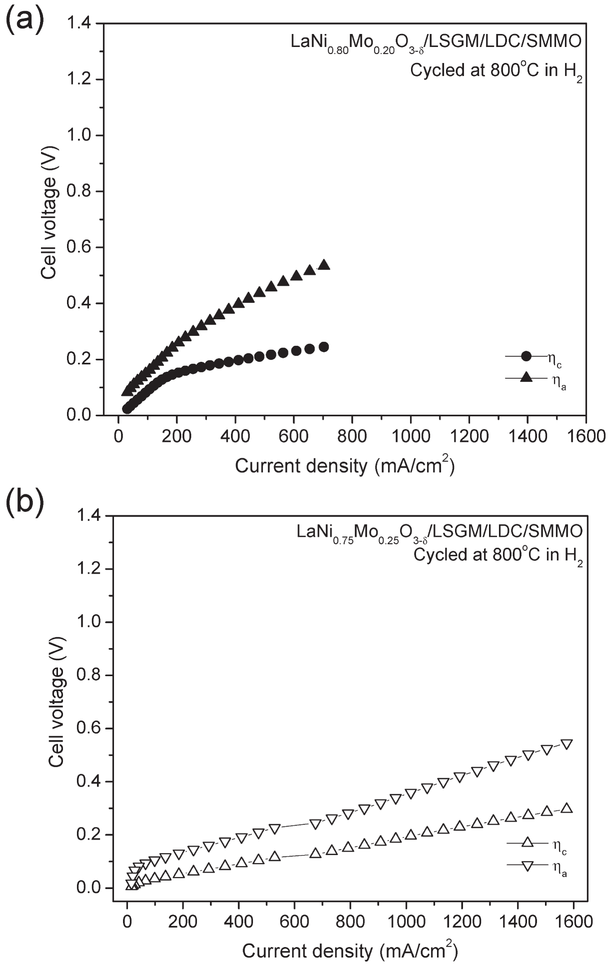

Figure 9. Anodic and cathodic overpotentials and open-circuit voltage for test cells with $LaNi_{1-x}Mo_xO_3$ (x = 0.20, 0.25) as cathodic materials.

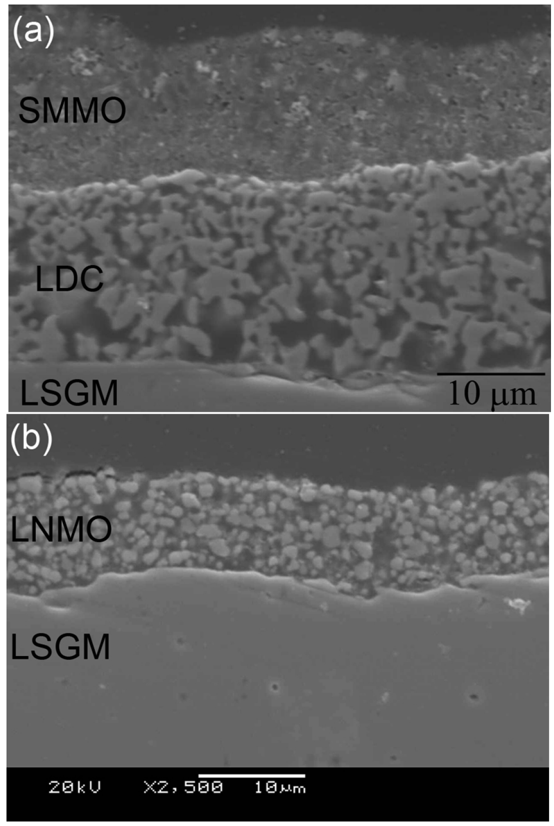

Figure 10. SEM images of a cross section of the test cell with (a) SMMO as anode and LDC as buffer layer and (b) $LaNi_{0.75}Mo_{0.25}O_3$ as cathodic material.

SMMO, and LNMO layers are estimated to be approximately 20, 15, and 10 μm, respectively. The cathode LNMO exhibits a fine and uniform microstructure with an estimated 30% porosity.

4. Discussion

Given its metallic behavior,[16] $LaNiO_3$ (containing Ni(III)) with an electronic conductivity of approximately 200 S cm^{-1} at 300 K[17,18] has always been considered a potential cathode material for SOFCs. Moreover, $LaNiO_3$ and related materials in the La−Ni−O system show excellent oxide-ion diffusion, potentially making them suitable for the first generation of cobalt-free commercial SOFCs.[19] In particular, $La_4Ni_3O_{10}$ (the n = 3 member of the Ruddlesden−Popper $(LaNiO_3)_n \cdot LaO$ series) has been reported to possess an excellent balance between ionic and electronic conductivity.[20] However, neither undoped $LaNiO_3$ nor $La_4Ni_3O_{10}$ can be utilized as successful cathodes in SOFCs given their instability in air atmosphere at the working temperature of an intermediate-temperature SOFC (typically 800 °C). These cathodes slowly lose oxygen, giving rise to mixtures of La_2NiO_4 (containing Ni(II)) and NiO.

In the $La_{1-y}Ni_{1-x}Mo_xO_{3-\delta}$ series of materials proposed in the present paper, the required long-term stability is achieved via chemical doping with sufficient amounts of Mo(VI) cations at the B sublattice of the perovskite structure. The introduction of Mo(VI) is very effective from this point of view because Mo cations are stable in 6-fold and 4-fold coordination, thus supporting the presence of a significant rate of oxygen vacancies in the structure. The Mo(VI) valence partially reduces the Ni(III) of $LaNiO_3$, thereby stabilizing the mixed-valent Ni(III)/Ni(II) couple against oxygen loss in air at 800 °C. Moreover, the oxygen vacancies undergo no long-range order. It is also important to note that Ni cations can also be stable in less than 6-fold oxygen coordination under certain conditions, as is shown in the paradigmatic example of $LaNiO_{2.5}$ where half of the Ni(II) cations are found in a square-planar coordination.[21] Both Ni and Mo cations can thus withstand the partial removal of oxygen required to incorporate O_2 molecules from the air and make possible the reduction process to O^{2-} oxide ions that can diffuse across the cathode and reach the surface of the electrolyte.

Our results demonstrate that lightly Mo-doped LNMO (x = 0.10 and 0.15) cathode materials in LSGM/SMMO fuel cells show a poor performance and degrade rapidly

(16) Goodenough, J. B.; Raccah, P. *J. Appl. Phys.* **1965**, *36*, 1031.
(17) Tiwari, A.; Rajeev, K. P. *J. Phys.: Condens. Matter* **1999**, *11*, 3291.
(18) Sreedhar, K.; McElfresh, M.; Perry, D.; Kim, D.; Metcalf, P.; Honig, J. M. *J. Solid State Chem.* **1994**, *110*, 208.
(19) Skinner, S. J.; Kilner, J. A. *Mater. Today* **2003**, *6*, 30.
(20) Zhang, Z.; Greenblatt, M. *J. Solid State Chem.* **1995**, *117*, 236.
(21) Alonso, J. A.; Martínez-Lope, M. J. *J. Chem. Soc., Dalton Trans.* **1995**, 2819.

during the first few power cycles. Apparently this level of Mo doping is not sufficient to stabilize LNMO under high temperature oxidizing conditions, and these lightly doped compounds resemble the behavior of undoped $LaNiO_3$ and are not suitable cathode materials for SOFCs, in spite of their remarkable electronic conductivity. However, the more heavily Mo-doped compounds, with nominal stoichiometries $x = 0.20$ and 0.25, may be considered as potential cathode materials in single test cells because they demonstrate superior maximum output powers of 330 mW/cm^2 for $x = 0.20$ and 630 mW/cm^2 for $x = 0.25$ at 850 °C in pure H_2. Moreover, a SOFC made from LNMO $x = 0.25$ showed a non-negligible power of approximately 565 mW/cm^2 at 800 °C, overcoming the requirements of 500 mW/cm^2 at 800 °C for practical use of a single cell. It also exhibited a good cyclability without apparent power loss up to 50 cycles. Its cathodic overpotential losses are smaller than the anodic ones, and therefore the cathodic losses are no longer rate-determining of the output power of the cell. Finally, the observed thermal expansion coefficient, of $\sim 9.8 \times 10^{-6}$ K^{-1}, is compatible with that of the electrolyte, between 11.4 and 12.1×10^{-6} K^{-1},[22,23] which decreases the possibility of cracking during fuel cell operation cycles.

We can correlate the observed performance with some structural aspects of the perovskite phases that constitute the major component of these cathode materials. Although structure analysis using in situ NPD at room temperature and 800 °C was performed on an LNMO sample with $x = 0.2$, the structural conclusions may also be applied to the LNMO $x = 0.25$ material given the similarity of their unit-cell parameters at room temperature determined and analyzed by X-ray diffraction studies (Section 3.1). LNMO $x = 0.20$ oxide displays at 800 °C a rhombohedral structure (space group $R\bar{3}c$) characterized by a moderate tilting of the octahedra (Ni−O−Ni ≈ 165°), which provides a good overlap between Ni 3d and O 2p orbitals and a high polaronic conductivity by hole hopping via Ni−O−Ni paths. The second important structural feature observed from NPD data at 800 °C is the significant oxygen deficiency: the crystal structure exhibits 0.22(2) oxygen vacancies per formula unit randomly distributed over the oxygen sites. The presence of disordered oxygen vacancies could account, by itself, for the necessary ionic conductivity of oxide anions that is required for the mass transport across the cathode. Moreover, an oxygen thermal factor of 2.9 Å^2, indicating a certain smearing of their nuclear density around their equilibrium positions, suggests a higher mobility for these atoms. Furthermore, the observed porosity of the cathode material (Figure 10) also contributes to a large surface area for oxygen reduction and transport of oxygen into the electrode.

The crystallographic formula $La_{0.984(6)}Ni_{0.88(3)}Mo_{0.12(3)}$-$O_{2.78(2)}$ for the $x = 0.2$ sample at 800 °C in air indicates a lower Mo content than expected from the nominal composition; it results from the presence of La_2MoO_6, of extraordinary thermodynamic stability, as a secondary phase. For this stoichiometry, we determine the Ni oxidation state to be 2.16+, which provides an adequate Ni(III)/Ni(II) valence mixing to permit good electronic transport via polaron hopping. The Ni valence of 2.27(1)+ obtained from bond-valence considerations[24,25] from the (Ni,Mo)−O distances is slightly biased by the presence of Mo(VI) (with an ionic radius of 0.59 Å, larger than that of low-spin Ni(III) in octahedral coordination, 0.56 Å[26]) over the same crystallographic positions.

Finally, the observation that the $x = 0.25$ material shows a better cathode performance than the $x = 0.20$ oxide under the same conditions although their crystal structures are extremely similar may be explained because the $x = 0.25$ perovskite contains a larger amount of La_2MoO_6 impurity phase. The segregation of La_2MoO_6, which has a high thermodynamic stability, requires the removal of La^{3+} cations from the main perovskite phase leading to La-defective compositions. The hole-doping effect induced by the substantial La deficiency enhances the stabilization of holes in the Ni(III)/Ni(II) couple in air atmosphere, thus boosting the electronic conductivity to give the better performance observed for this material as a cathode in the test cell. In fact, the conductivity curves of the $x = 0.20$ and $x = 0.25$ phases undergo a crossover at 450 °C (Figure 5a), which confirms our hypothesis and implies a slightly better electronic transport for the $x = 0.25$ phase. Trials to prepare a cathode material designed with the nominal composition $La_{0.8}Ni_{0.8}Mo_{0.2}O_3$ did not produce a single phase but a mixture of the main perovskite phase with La_2MoO_6 and NiO; the performance of this material as cathode in a test cell was similar to that of the original $x = 0.20$ sample. The formation of a La-deficient perovskite with the required properties was more effective via segregation of La_2MoO_6, which promotes the creation of La vacancies in the early stages of the synthesis of the perovskite phase.

5. Conclusions

We have designed, characterized, and tested defective Ni perovskites of composition $La_{1-y}Ni_{1-x}Mo_xO_{3-\delta}$ as cathode materials for intermediate-temperature SOFCs with long-term stability and competitive power performance in the temperature range 750−850 °C. The Ni(III) of $LaNiO_3$ is reduced to Ni(II) by oxygen loss at the operating temperature of an intermediate-temperature SOFC. Introduction of Mo(VI) would reduce Ni(III) to Ni(II) even if it were not accompanied by the creation of oxygen vacancies. The segregation of La_2MoO_6 from nominal $LaNi_{0.75}Mo_{0.25}O_{3-\delta}$ introduces La vacancies that partially reoxidize Ni(II) to give mixed valence in the Ni(III)/Ni(II) couple at 800 °C in air while leaving enough Mo(VI) to provide randomly distributed oxygen vacancies. The result is a competitive, cobalt-free cathode

(22) Naiqing, Z.; Kening, S.; Dewi, Z.; De Chang, J. *J. Rare Earths* **2006**, *24*, 90.
(23) Lee, D.; Han, J. H.; Chun, Y.; song, R. H.; Shin, D. R. *J. Power Sources* **2007**, *166*, 35.
(24) Brese, N. E.; O'Keeffe, M. *Acta Crystallogr., Sect. B* **1991**, *47*, 192.
(25) Brown, I. D. *Z. Kristallogr.* **1992**, *199*, 255.
(26) Shannon, R. D. *Acta Crystallogr.* **1976**, *A32*, 751.

material that meets the power-density target for an intermediate-temperature SOFC.

Acknowledgment. We are grateful to ILL for making the beamtime available. J.B.G. thanks the NSF and the Robert A. Welch Foundation of Houston, TX, Grant F-1066, for financial support. J.A.A. and M.J.M.-L. acknowledge the financial support of the Spanish "Ministerio de Ciencia e Innovación" to the project MAT2007-60536 and during his sabbatical.